Ceramics International 48 (2022) 5724–5736

Contents lists available at ScienceDirect

Ceramics International

journal homepage: www.elsevier.com/locate/ceramint

The use of Mount Etna volcanic ash in the production of bricks with good physical-mechanical performance: Converting a problematic waste product into a resource for the construction industry

Giuseppe Cultrone

Department of Mineralogy and Petrology, Faculty of Sciences, University of Granada, 18002, Granada, Spain

ARTICLE INFO

Keywords:
Volcanic ash
Brick production
Petrophysical behaviour
Technical quality

ABSTRACT

Volcanic ash emissions are responsible for serious damage to buildings. They can also affect vehicle traffic, cause airport closures and may be hazardous for human health. To verify the effects of the potential addition of this residue to the mixture used in the production of bricks, a detailed study of the clayey material, the volcanic ash and the bricks fired at 800, 950 and 1100 °C was conducted, assessing chemical, mineralogical, physical, mechanical and durability aspects. The addition of 10–20 wt% of volcanic ash delayed the appearance of new phases during brick firing and made them less porous. The bricks maintained their orange colour and became more compact as the firing temperature increased due to sintering and vitrification processes. The addition of volcanic ash reduced the strength of the bricks although the values were always above the limits recommended for construction work with ceramic materials. Bricks with added volcanic ash increased their resistance to decay due to salt crystallization and the general behaviour of the bricks improved when they were fired at high temperatures.

1. Introduction

Etna, in eastern Sicily (Italy), is one of the most active volcanoes in the world. It is a basaltic stratovolcano whose activity takes place from the four summit craters and, less frequently, from fissures opened on the flanks of the mountain, alternating explosive activity (strombolian and/or lava fountains) with lava flows [1–3]. Generally, volcanism lasts from two to four weeks, although periods of activity lasting over six months or just a few hours have also been recorded [4]. The local landscape is strongly influenced by the presence of Mount Etna, above all in the summit area whose morphology is changed by each eruption [5,6]. The volcano has also affected many aspects of human life in the towns and cities situated around it. Many of their historic monuments from the Roman age to the Baroque were erected with basalt quarried from the flanks of Mount Etna.

In recent decades, changes in the characteristics of the eruptions have led to major emissions of volcanic ash [2]. The extent to which the ash is scattered is influenced by the height of the plume, the duration of the eruption and the prevailing winds [7]. Volcanic ash outcrops are not exclusive to the Etna area and can be found in many regions of the world affected by volcanic activity past or present. Their chemical and mineralogical composition varies according to the composition of the magma from which they originate. Ash fall can cause serious damage to infrastructure networks and structural damage to buildings due to the large accumulation of particles on roofs or reduced traction on roads or airport runways. This ash must therefore be removed as part of the proper maintenance of urban areas [8]. Moreover, exposure to volcanic ash is potentially hazardous for human health because it can cause respiratory problems and/or eye or skin irritations [9,10]. It can also contaminate aquifers due to the leaching of metals from ash particles in prolonged contact with water [11,12]. If the ash is not removed, it can cause further health complications as the particles can be remobilized by wind and vehicle traffic [7].

In addition to the aforementioned problems, another important issue is how to dispose of waste of this kind, given that for example, the cultivated and inhabited areas around Mount Etna can receive several kg/m^2 of ash during an eruption [13].Volcanic ash is currently disposed of in landfills and there is no clear legislation regarding its disposal and recycling. The European Union classifies volcanic ash within the generic group of "Municipal residues" (code 20) and more specifically as "street-cleaning residues" (code 0303).

Several studies have analysed the reuse of volcanic ash as an additive for various building materials, especially mortars and concretes. However, when the ash does not show pozzolanic activity only larger

E-mail address: cultrone@ugr.es.

https://doi.org/10.1016/j.ceramint.2021.11.119
Received 23 September 2021; Received in revised form 29 October 2021; Accepted 13 November 2021
Available online 17 November 2021

particles can be used as aggregates [14,15]. Another possible application is in the synthesis of geopolymers based on their aluminosilicate content or to improve the quality of untarred roads [16,17]. A recent review carried out by Lemougna et al. [18] (and references therein) highlighted, among others, the potential use of volcanic ash in the production of Lunar and Martian soil simulants, in order to facilitate the development of structural materials with a similar composition for habitat constructions outside our planet.

A large number of organic and inorganic wastes have been tested for their possible use as additives in the manufacture of ceramic products [19–24]. However, volcanic ash has rarely been used for this purpose. It has been detected in archaeological artefacts made in places with volcanoclastic sediments used as raw material. Examples include Maya ceramics from the archaeological site of Tierra Blanca in Mexico [25] or Roman ceramic pieces from Cuma in the Bay of Naples in Italy [26].

Some specific studies into the use of volcanic ash have been made. These include for example the study by Serra et al. [27], who verified the possibility of replacing K-feldspar with milled volcanic ash as a flux agent in the production of porcelain stoneware or other white-type ceramics, obtaining promising results. Vu et al. [28] mixed weathered volcanic ash and waste glass, which they ground down and fired at 800 and 815 °C to obtain porous ceramics that could be used to control the humidity of building walls. No clayey materials were used in the making of these ceramics. Belfiore et al. [29] tested 20 vol% sieved volcanic ash with a clayey material in the manufacture of ceramic tiles obtaining similar physical and mechanical results as other more standardized products.

The purpose of this research is to verify the possibility of recycling volcanic ash in the production of solid bricks to obtain two main benefits: firstly, a reduction in the use of non-renewable resources, such as clayey materials, which are used in significant amounts by the ceramic industry; and secondly, protecting the environment and human health by trying to eliminate or at least reduce volcanic ash accumulation in landfills. Both benefits are part of the first of the European Commission's six priorities for 2019–2024, in what they dub as "A European Green Deal" to ensure sustainable industry with "more environmentally friendly production cycles" (https://ec.europa.eu/info/strategy).

Although, as mentioned above, researchers have tested the possibility of using volcanic ash as an additive in the production of ceramics, it has never been used as an additive in bricks. The products technologically closest to bricks in which volcanic ash was used in this way were the tiles investigated by Belfiore et al. [29]. However, prior to adding the ash, they manipulated it by sieving it. They did not test different percentages of ash and only fired the tiles at one temperature. In the following section, a different methodological approach for brick production (raw material, waste amount, firing temperatures and firing process) is described.

2. Materials used and geological setting

The raw material used to manufacture the bricks was provided by a brick factory (Ceramica Castillo Siles, S.L., Viznar, Spain), who mix two clayey soils to create the raw material for their products. One soil is from Viznar and the other from Guadix (Granada, Spain) and they are mixed together in the following proportions: 4/5 Viznar and 1/5 Guadix (by volume). The raw materials from Viznar and Guadix are geologically located in the Granada basin and Guadix-Baza basin, respectively. These basins are the largest intramontane depressions in the Betic Cordillera, which formed during and after the Upper Miocene. The oldest materials from the two basins date from the Tortonian age, while the most recent date from the Middle Pleistocene (in the Granada basin) [30,31] and the Late Pleistocene (in the Guadix-Baza basin) [32]. During the Holocene and probably during part of the Upper Pleistocene, there were erosion and sedimentation processes linked to the current river system [33]. The raw material quarried in Viznar comes from the silty levels dating from the Pliocene that outcrop close to the city of Granada, while the raw material from Guadix comes from the clayey sediments in the Guadix Formation, which is made up of detrital materials from the Plio-Pleistocene age.

As regards the provenance of the volcanic ash used as an additive in the brick production, a long phase of strombolian activity began in the middle of August 2020, producing a dark ash column from the new SE crater of Mount Etna. The column varied in intensity and explosions until the end of the month, causing fallout in the direction of the nearby city of Catania (as reported in Volcano Observatory Notices for Aviation: www.ct.ingv.it). The volcanic ash, which is dark grey-black in colour, was collected at the end of August in Contrada Ronzini, a district of Trecastagni (province of Catania).

3. Preparation of the samples and firing process

The raw material (4/5 Viznar + 1/5 Guadix) was milled and sieved, and the fraction of over 2 mm was discarded, in a similar procedure to that applied in the brick factory. 10% and 20% volcanic ash was added "as collected" (i.e., it was not ground or sieved). The addition was by weight. With volcanic ash, there is almost no difference between weight percent and volume percent added and the addition by weight allows for easier comparison with other waste products found in the literature [20,22]. The possibility of using higher percentages of volcanic ash was discarded to ensure that the bricks retained the right consistency [29]. The raw material and the waste (when present) were mixed homogeneously by hand and then water was added. The samples were prepared manually because the brick factory that supplied the raw material makes its own bricks with both industrial (by extrusion) and artisanal production methods. There is growing demand for the latter, which are often used in the cladding of houses with a rustic finish as well as in the restoration of historic buildings. 330 ml of water was added per 1000 g of raw material to make the samples with no additive. When the volcanic ash was added less kneading water was required, saving 7% and 14% of water with 10% and 20% of waste, respectively. When the mixture was sufficiently plastic, a wet wooden mould measuring 4 × 12 × 16 cm was filled. The mixture was compacted by pressing down firmly by hand. The top of the mould was smoothed off with a ruler to obtain a flat, even surface. After half an hour the mixture was compact enough and the mould was removed. A tense nylon thread was used to cut the raw piece into cubes with approximately 4 cm-edge and each piece was separated from the others to enable them to dry more effectively. When the drying was complete (about a week later), the edges of the cubes were smoothed with a file to remove roughness.

The bricks were fired in a Herotec CR-35 electric oven with oxidation atmosphere. The samples were kept for 1 h at 100 °C in order to remove any dampness that might still be present in the unfired samples. Samples were then fired at 800, 950 and 1100 °C with a heating speed of 2 °C/min. Once the maximum temperature was reached, it was maintained for 3 h. Finally, the oven was switched off to allow the bricks to cool. The entire firing-cooling process took 24 h. When the bricks were removed from the kiln, they were immersed in water for about half an hour to prevent "lime blowing" in the event that there were carbonate grains in the raw material [34]. Nine types of bricks were prepared, combining the three firing temperatures and the three mixtures: i) raw material with no added volcanic ash, ii) with 10 wt% of volcanic ash, and iii) with 20 wt% (Table 1).

Table 1
Acronym assigned to each brick group based on the amount of volcanic ash (in wt.%) and the firing temperature.

Volcanic ash	800 °C	950 °C	1100 °C
0	VG800	VG950	VG1100
10	VGa800	VGa950	VGa1100
20	VGb800	VGb950	GVb1100

4. Experimental procedure

4.1. Granulometry and petrochemical characterization

The granulometry of the clayey raw material and of the volcanic ash was defined using a Malvern Instruments Matersizer 2000LF apparatus, which used laser diffraction to measure the size of the particles (within the 0.02 μm - 1.5 mm range of the apparatus) after 10 s sonication in water.

The chemistry (major and trace elements) of the raw material and of the volcanic ash was determined by X-ray fluorescence (XRF) using a PANalytical Zetium compact spectrometer with a Rh anode and a 4 kV X-ray generator. 7 g per sample were milled to powder in an agate mortar and then analysed.

The mineralogy of the raw material, the volcanic ash and the fired bricks was determined by means of powder X-ray diffraction (PXRD) using a PANalytical X'Pert PRO diffractometer with a CuKα radiation (λ = 1.5405 Å) and operating at 45 kV and 40 mA. The samples were analysed between 4 and 70° 2θ with a goniometer speed of 0.01 2θ/s. The samples were milled in an agate mortar to a particle size of less than 53 μm and then analysed. PXRD analysis of the fraction below 2 μm was performed on oriented aggregates, which were air-dried (OA), solvated with ethylene-glycol at 60 °C for 48 h (OA + EG) [35], and heated to 550 °C for 90 min (OA + 550 °C) [36] to identify the clay minerals present in the raw material. Carbonates were eliminated from the raw material by adding 0.2 N acetic acid (CH_3COOH) solution, while any possible organic matter was removed by adding hydrogen peroxide (H_2O_2) at 20 vol%. After that, sodium hexametaphosphate ($Na_6P_6O_{18}$) was added to separate any aggregates that might have formed and the clay fraction was separated from coarser fractions using a Kubota 2000 centrifuge. The HighScore software v.4.8 (Malvern Panalytical) was used to process the PXRD patterns and to identify mineral phases by matching the experimental diffraction patterns to those included in the COD database (www.crystallography.net/cod/).

The thermal decomposition of the raw material from Guadix was studied by means of thermogravimetry (TG) and Differential Scanning Calorimetry (DSC). TG/DSC analysis was performed in the 25–950 °C temperature range using a Mettler-Toledo TGA/DSC1. 20 mg of powdered sample was placed on an Al crucible and heated at a rate of 20 °C/min in a flowing air atmosphere (50 ml/min).

The microscopic identification of the mineral phases and of the texture of the bricks with and without added volcanic ash was observed on thin sections under a polarized optical microscope (POM, Carl Zeiss Jenapol-U). The microscope lens is connected to a Nikon D7000 digital camera to save images in plane- and crossed-polarized light.

The appearance of the volcanic ash and the microstructural features of the bricks were studied in detail using a field emission scanning electron microscope with a focused ion beam (FESEM) Carl Zeiss STM (AURIGA Series) with EDS microanalysis. The ash particles and brick fragments were carbon-coated prior to this analysis.

4.2. Physical properties

To assess the hydric behaviour of bricks, free (A_b), forced (under vacuum) water absorption (A_f) and drying (Di) tests were performed following UNE-EN 13755 [37] and NORMAL 29/88 [38] standards using deionized water. These tests allowed us to calculate the degree of pore interconnection (Ax) [39], the saturation coefficient (S), the apparent (ρ_a) and real densities (ρ_r) and the open porosity (Po) according to the RILEM standard [40]. Three samples per brick group were analysed under controlled thermo-hygrometric conditions (18 °C and 35% relative humidity).

The porous system of the bricks was then analysed in more detail with mercury intrusion porosimetry (MIP) using a Micromeritics Autopore IV 9500 porosimeter. The pore size distribution was examined within the 0.002–200 μm range. One sample per brick type of about 1 cm^3 was oven-dried at 70 ± 5 °C for 8 h before being analysed.

The compactness of the bricks was evaluated by ultrasound, a non-destructive technique that assesses the strength of materials and analyses their structural anisotropy [41,42]. A Controls 58-E4800 ultrasonic pulse velocity tester was used together with transducers with a contact surface of 3 cm in diameter and a frequency of 54 kHz. Three samples per brick type were measured. The propagation of P-waves was measured in the three orthogonal directions using the direct method in accordance with the ASTM D2845 standard [43] on dry samples. The anisotropy (ΔM) was calculated according to the following equation [43]:

$$\Delta M = \frac{V_{max} - V_{min}}{V_{max}} \times 100$$

where V_{max} and V_{min} are respectively the maximum and minimum velocities measured in bricks regardless of the measurement direction.

The strength of the bricks was also measured using the uniaxial compression test. The mechanical test was carried out using a Matest Press Test E181, which can exert a maximum load of 250 kN. The analysis was conducted on three samples per brick type according to the UNE-EN 1926 standard [44]. The surfaces of the cubic samples were previously smoothed with a cutting disk in order to obtain perfectly plane and parallel surfaces. Compression strength was measured perpendicular to the compaction plane of the raw mixture in the wooden box.

Another non-destructive technique, spectrophotometry, was used to measure the colour of the brick and to quantify the colour difference (ΔE), due to the addition of volcanic ash. A portable Konica Minolta CM-700d apparatus was used in accordance with the UNE-EN 15886 standard [45]. A CIE illuminant D65 that simulates daylight with a colour temperature of 6504 K was selected to measure the lightness (L*), chromatic coordinates (a* and b*), chroma (C*) and hue angle (h°) in the 400–700 nm wavelength range. A pulsed xenon lamp with a UV cut filter was used to illuminate a circular area of the bricks with a diameter of 8 mm (10° vision angle). The light was measured with a silicon photodiode array in SCI and SCE modes. Three measurements were made per brick type. The ΔE was calculated as follows:

$$\Delta E = \sqrt{\left(L_1^* - L_2^*\right)^2 + \left(a_1^* - a_2^*\right)^2 + \left(b_1^* - b_2^*\right)^2}$$

where L_1^*, a_1^*, b_1^* are the lightness and chromaticity values for the bricks made without additive and L_2^*, a_2^*, b_2^* for those made with added volcanic ash.

4.3. Durability

The bricks were subjected to the salt crystallization test following the UNE-EN 12370 standard [46]. This accelerated ageing test provides information on the damage produced by soluble salts when they crystallize in pores and fissures. 15 cycles were performed on three bricks of each type using a 14% $Na_2SO_4 \times 10H_2O$ solution. The deterioration of the bricks was assessed by measuring the weight and observing any loss of fragments.

5. Results and discussions

5.1. Macroscopic observations

The addition of volcanic ash not only reduced the amount of kneading water required but also the shrinkage of the samples after drying. While the bricks made without the additive shrunk by 8%, those made with 10% volcanic ash shrunk by 6.5% and those made with 20% volcanic ash shrunk by just 4.3%. The reduction in shrinkage due to the addition of volcanic ash was expected given that volcanic ash is a non-plastic material and acts like a temper. The size of the bricks was

unaffected by the firing process.

5.2. Composition and characteristics of the raw materials

In chemical terms, the raw material used to manufacture the bricks is rich in silica (46 wt%) and has considerable amounts of alumina (15 wt %) and calcium (10 wt%). Iron and magnesium appear in smaller amounts. The loss on ignition (LOI, Table 2) is just over 14 wt% and may be due to the decomposition of carbonates, the dehydroxylation of phyllosilicates and the combustion of organic matter. The raw material can be classified as calcareous given that its calcium content is over 6% [47]. Among the trace elements Ba, Sr, Zr and V prevail (Table 2).

The volcanic ash has almost the same levels of silica, alumina, calcium and magnesium. However, it is richer in iron (12.1 wt%) and sodium (3.2 wt%) (Table 2). It also has more than twice as much TiO_2 as the raw material. The most abundant trace elements in the clayey material are the same as in volcanic ash, although they (especially Sr) appear in greater concentrations in the latter. Based on the Total Alkali-Silica diagram [48], the volcanic ash can be classified within the group of trachybasalt rocks, next to that of basalts. This classification is similar to the composition of volcanic products from Mount Etna found in the literature [49]. The LOI content is almost null which means that the calcium detected in the volcanic ash cannot be due to the decomposition of carbonates and could be linked to the presence of Ca silicates.

This assumption is confirmed by the results of the mineralogy analysis by PXRD. In fact, the volcanic ash is rich in Ca-plagioclase (Fig. 1a). It also presents smaller quantities of augite and olivine and traces of Ti-magnetite, which explain the high iron content and the presence of titanium. This mineralogy is typical of the basaltic rocks of Mount Etna [50–52].

The raw material is rich in quartz and also contains phyllosilicates and carbonates (calcite and dolomite) (Fig. 1b). The analysis of the fraction below 2 μm highlighted that the phyllosilicates are composed of illite, smectite and small amounts of chlorite, kaolinite and paragonite (Fig. 1c). Paragonite is a relatively rare clay mineral that is produced by the erosion and transport of metamorphic rocks from Sierra Nevada [53]. The disappearance of the d_{001} peaks of smectite at about 12.5 Å and kaolinite at about 7.2 Å after heating the oriented aggregate to 550 °C revealed the presence of chlorite (Fig. 1d). After treatment with EG, the d_{001} peak of smectite expanded, as can be observed by the displacement of the diffraction line at 16.7 Å, which confirms the presence of swelling clay minerals (Fig. 1e).

The results of the thermogravimetry (TG) and Differential Scanning Calorimetry (DSC) analyses of the raw material are presented in Fig. 2. There is an initial endothermic peak in the DSC curve with a minimum at 80 °C that corresponds to the loss of hygroscopic water. A further two peaks at 206 °C and 290 °C are related to the combustion of labile organic matter [54]. Other endothermic peaks were registered at 412 °C, 531 °C and 606 °C. All of them correspond to the dehydroxylation of phyllosilicates. According to the mineralogy determined by PXRD, the first peak can be attributed to the loss of structural water in low crystalline phases (i.e., those with a broad Bragg peak in the PXRD pattern) such as smectite. The second peak may be due to the dehydroxylation of chlorite and kaolinite, whereas the most crystalline clays, namely illite and paragonite, dehydroxylate around 600 °C [55,56]. The greatest weight loss is observed in the DSC curve with a minimum endothermic peak at 806 °C and in the TG curve, which has quite an important step at the same temperature and a weight loss of 11.5%, due to the decomposition of carbonates and the release of CO_2. Another small endothermic peak can be seen at 870 °C due to the continuing release of the remaining OH^- present in the illite/muscovite [57]. The total weight loss measured by the TG curve is 16.24%, which is very similar to that measured by chemical analysis (LOI, Table 2).

In terms of grain size, the clayey material (VG) has a particle-size distribution between 1 and 200 μm with a maximum peak at around 20 μm and a second smaller, but wider, interval and a peak at 1500 μm. The volcanic ash (va) is almost unimodal and is characterized by coarser particles with a maximum peak at 150 μm, most of which are between 50 and 450 μm (Fig. 3a).

The ash particles consist of tachylite. They show smoothed, poorly vesicular surfaces with conchoidal fractures (Fig. 3b). Occasionally and in line with PXRD analysis, crystals of Ca-plagioclase and Ti-magnetite have been identified (Fig. 3c).

5.3. Characteristics of the fired bricks

5.3.1. Mineralogy

After firing, the bricks undergo significant mineralogical changes. At 800 °C the bricks made without additives (VG800) are rich in quartz and still contain calcite, albeit in smaller amounts than the raw material, while the dolomite has disappeared (Table 3). Of all the phyllosilicates identified in the raw material, only the illite/muscovite remains. There are small peaks of plagioclases and the iron in the raw material has crystallized as hematite. At this temperature, a new silicate phase, gehlenite ($Ca_2Al_2SiO_7$), has developed. This phase is formed after the reaction between phyllosilicates, quartz and calcite [55]. At 950 °C (VG 950), the peak of illite/muscovite descends as it becomes involved in the formation of gehlenite, which, by contrast, shows an increase in quantity (Table 3). It is surprising to find calcite at this temperature, albeit in traces, as it should have completely decomposed [58,59]. However, other researchers have identified calcite in ceramics fired at higher temperatures [60]. The relatively short firing times of the bricks, the calcite grain size and, above all, the increase in the CO_2 partial pressure in the oven during firing can result in a slower calcite decomposition process [61–63]. There is an increase in the amount of plagioclase which now has a higher calcium content, while the quartz content remains almost unchanged. At 1100 °C (VG1100), two other new silicates, diopside ($CaMgSi_2O_6$), and mullite ($Al_6Si_2O_{13}$) appear (Table 3). Diopside is produced by the reaction between quartz and dolomite [55], while mullite replaces the illite/muscovite [57]. The amount of quartz falls due to its continued involvement in the formation of gehlenite and Ca-plagioclase, while the plagioclase content rises, turning into anorthite. There is a rise in the amorphous phase between 800 and 1100 °C. This can be deduced from the increase in background noise in the

Table 2
Chemical analysis of major oxides (in wt.%) and trace elements (in ppm) in the mixed raw material from Viznar and Guadix (VG) and the volcanic ash from Mount Etna (va). LOI stands for loss on ignition.

	SiO_2	Al_2O_3	Fe_2O_3	MnO	MgO	CaO	Na_2O	K_2O	TiO_2	P_2O_5	LOI
VG	46.03	15.02	5.64	0.07	4.31	10.02	0.54	2.68	0.78	0.12	14.34
va	47.06	16.12	12.12	0.17	6.05	10.79	3.16	1.84	1.81	0.50	0.50
	Zr	**Sc**	**V**	**Cr**	**Co**	**Ni**	**Cu**	**Zn**	**Ga**	**Rb**	**Sr**
VG	184.3	11	107	86	14	39	23	72	16	99	248
va	217.6	18	309	35	36	21	133	107	20	47	1160
	Y	**Nb**	**Sn**	**Ba**	**La**	**Ce**	**Nd**	**Pb**	**Th**	**U**	**Cs**
VG	22	11	3	393	38	71	32	23	8	2	7
va	26	42	3	721	73	135	57	15	7	5	0

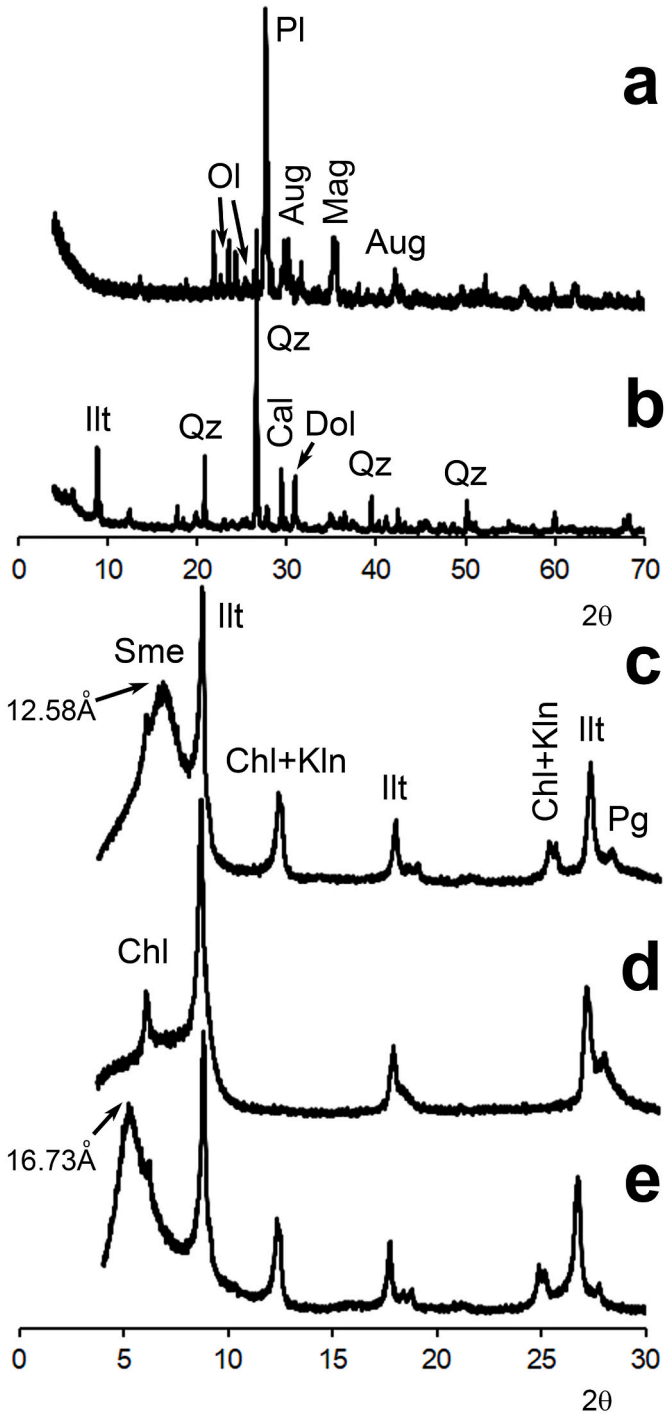

Fig. 1. PXRD diagrams of the volcanic ash (a), the raw material (b) and oriented aggregates from the clay fraction (c, d and e). These aggregates are: air dried (c), heated at 550 °C (d), and treated with ethylene-glycol (e). Legend: Pl = Ca-plagioclase; Aug = augite; Ol = olivine; Mag = Ti-magnetite; Qz = quartz; Cal = calcite; Dol = dolomite; Sme = smectite; Ilt = illite; Chl = chlorite; Kln = kaolinite; Pg = paragonite. Mineral abbreviations after Whitney and Evans [79].

diffractograms and suggests that the bricks are becoming increasingly vitrified. The addition of volcanic ash seems to delay the development of reaction phases at least at low firing temperatures. In fact, at 800 °C, even though the dolomite has disappeared, calcite does not yet appear to be involved in the reaction with silica and no new silicates have formed in either VGa800 or VGb800 bricks (Table 3). The addition of a flux agent (i.e., volcanic ash) seems to hinder the migration of CO_2 towards

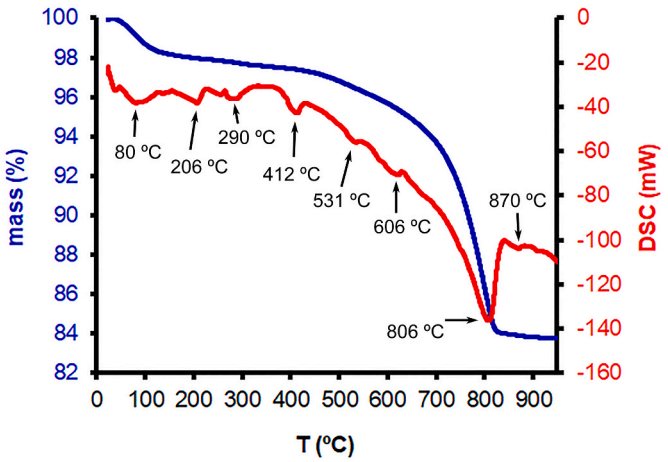

Fig. 2. TG (blue) and DSC (red) curves for the raw material used to manufacture the bricks. (For interpretation of the references to colour in this figure legend, the reader is referred to the Web version of this article.)

the outside even more than in the bricks made without additive. This leads to an increase in CO_2 partial pressure, which inhibits the decomposition of calcite [61]. There is more plagioclase in VGb800 than in VGa800 due to its higher added ash content (20 wt%), which is rich in this tectosilicate. This higher ash content also causes VGb800 bricks to show higher background noise. At 950 °C, calcite is still present albeit in decreasing amounts. This reduction is accompanied by the appearance of gehlenite, which is more abundant in VGb950. At this temperature, the plagioclase content is somewhat higher than at 800 °C and clinopyroxene peaks are clearly distinguishable in VGb950. Given the superposition of the augite and diopside diffraction lines, it is difficult to distinguish between the two. In this case, it seems more likely that the peaks are due to the augite present in the volcanic ash than to the newly formed diopside, as they do not appear in the diffraction patterns of the VGa900 bricks. At 1100 °C, the differences between bricks with and without additives are negligible. The ions are highly mobile which favours the incorporation of all the available Ca in the formation of new silicate phases. Even if the amounts of plagioclase and clinopyroxene appear to be higher in VGa and VGb bricks compared to VG, this is because these phases were already partly present in the volcanic ash (Table 3).

5.3.2. *Texture*

Observations under optical (POM) and electron (FESEM) microscopes were only conducted in the bricks without additive and in those with 20 wt% volcanic ash, in order to highlight the textural differences produced by the addition of the residue.

POM images show that the bricks without additives that were fired at 800 °C are characterized by a reddish matrix in which the grains are mainly composed of irregularly-shaped gneiss fragments, of up to 1.5 mm in size and with typical grano-lepidoblastic texture in which equigranular quartz grains alternate with thinner bands of muscovite-type mica (Fig. 4a). Fragments of mica schists are less frequent. Quartz can also be observed as isolated grains with irregular edges and undulose extinction. The interference colour of muscovite can reach second order blue (Fig. 4a). In addition to quartz, the non-plastic part of the bricks is also composed of calcite and rare feldspar fragments. The calcite grains are grey in colour but inside the crystals, they still show their typical interference colour, albeit irregularly and in patches, indicating that the decomposition process has not yet been completed (Fig. 4b).

At 950 °C the matrix is still red although it has a slightly darker hue. The calcite has now decomposed assuming a uniform grey colour. Muscovite-type phyllosilicates are losing their birefringence, acquiring a generalized first order yellow-red interference colour (Fig. 4c).

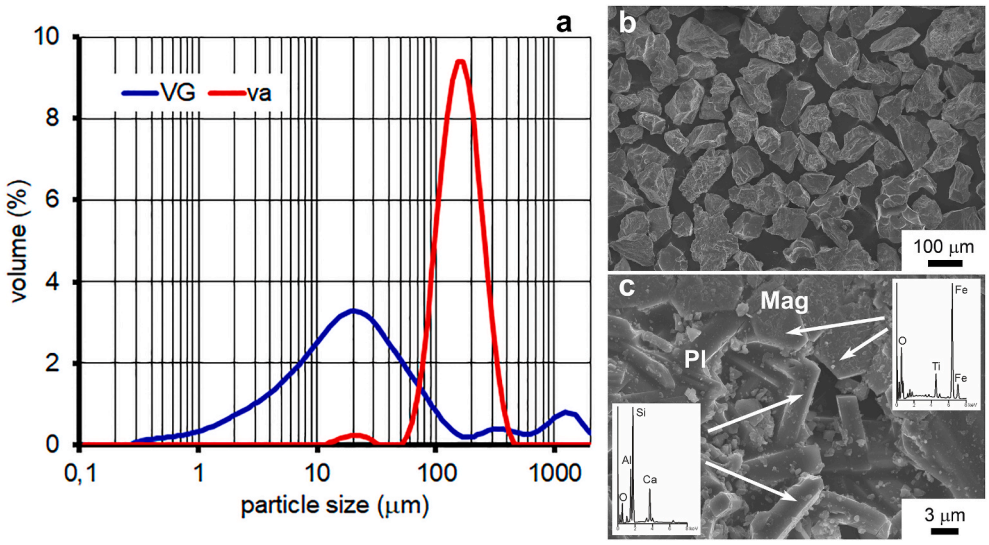

Fig. 3. a) grain-size distribution curves for the clayey material (VG) and the volcanic ash (va); b) general view of ash particles under FESEM; c) detailed image of a fragment in which Ca-plagioclase (Pl) and Ti-magnetite crystals (Mag) have been identified (see EDS spectra). Mineral abbreviations after Whitney and Evans [79].

Table 3
Mineralogical composition by PXRD of fired bricks. Legend: Qz = quartz; Ilt = illite/muscovite; Cal = calcite; Hem = hematite; Pl = Na–Ca plagioclase; Gh = gehlenite; Cpx = clinopyroxene (diopside and augite). *** = very abundant; ** = abundant; * = scarce; tr = in traces. Mineral abbreviations after Whitney and Evans [79].

	Qz	Ilt	Cal	Hem	Pl	Gh	Cpx	Mul
VG800	***	**	*	tr	*	*		
VG950	***	*	tr	*	**	**		
VG1100	**			*	***	**	**	*
VGa800	***	**	**	tr	*			
VGa950	***	**	*	*	**	tr		
VGa1100	**			*	***	**	***	*
VGb800	***	**	**	*	**		tr	
VGb950	***	**	tr	*	**	**	*	
VGb1100	**			*	***	**	***	*

At 1100 °C the bricks undergo major textural changes. The matrix now appears uniform and compact. It has turned yellowish and has lost birefringence due to vitrification (Fig. 4d). The phyllosilicates have acquired a first order white interference colour and, according to Rodriguez Navarro et al. [57], have probably been replaced by mullite. Indeed, PXRD analysis highlighted the absence of muscovite and the appearance of mullite at this temperature (Table 3). Carbonates are no longer present, while small red hematite crystals are scattered around inside the yellow matrix (Fig. 4d).

When volcanic ash is added, the main textural difference is precisely the presence of these black particles of volcanic glass inside which crystals of albite twinning plagioclase, augite-type pyroxene and, less frequently, olivine can be seen. At 800 °C, the other phases identified - quartz, phyllosilicates and carbonates – look very similar to those observed in the bricks without additive (Fig. 4e). It is interesting to see that calcite is still evident at 950 °C, especially in the highly birefringent internal areas of the crystals, so confirming the results of PXRD (see Table 3), i.e. that the carbonate has not completely decomposed at this temperature (Fig. 4f). The fact that the decomposition of some phases and the development of others is somewhat slower in the bricks with added volcanic ash is also confirmed by the interference colours of the muscovite crystals, which maintain a second order blue colour at this temperature (Fig. 4g). At 950 °C and above all at 1100 °C the edges of the volcanic particles are no longer clearly defined and instead appear diffused within the matrix of the bricks, suggesting that they have melted at least partially and are perfectly bonded to the matrix (Fig. 4h). Quartz, low birefringent phyllosilicate (maybe mullite) and the phases inside the volcanic ash (plagioclase, pyroxene and olivine) can still be identified in a yellowish matrix.

Under FESEM, at 800 °C, the laminar morphology of the phyllosilicates remains, although marked exfoliation along the (001) plane is evident due to dehydroxylation (see white arrow, Fig. 5a). The quartz has an angular morphology and the pores are irregularly shaped. There is no evidence of partial melting of the clay matrix at this temperature. At 950 °C, the bonding between the particles increases, although the pores are still irregular in shape (Fig. 5b). It is possible to observe the remains of ancient carbonate grains composed of nanometric MgO and CaO grains which have probably undergone sintering [64], together with the formation of new silicates (e.g., gehlenite, see EDS spectra) (Fig. 5c). At 1100 °C, the texture of the bricks undergoes profound change: the surfaces are smoother and the pores coalesce and become larger, acquiring rounded or ellipsoidal shapes (Fig. 5d). The bond between the particles is stronger, making the structure more compact. The addition of volcanic ash is clearly visible at 800 °C (Fig. 5e and EDS spectrum of a silicate glass). It is perfectly bonded to the clay matrix but there is no evidence of even partial melting. At 950 °C there seem to be fewer ash fragments than in the bricks fired at 800 °C. This means that the additive must have partially melted within the structure of the bricks. Grains of decomposed carbonates are scattered here and there in the clay matrix (see white arrow, Fig. 5f). At 1100 °C, the matrix of the bricks made with volcanic ash is fully vitrified and has a very similar appearance to that of the bricks made without additives: the pores are rounded, the grain boundaries become smooth and are well joined together. Volcanic ash fragments are no longer observed (Fig. 5g).

5.3.3. *Pore system*

Fig. 6 shows the average values for free and forced water absorption and for drying for the three groups of bricks fired at 800, 950 and 1100 °C. At first glance, the free absorption curves (part 1 of Fig. 6) for the samples without additive (green curves) appear to absorb more water than those with 10 wt% volcanic ash (red curves) and these in turn absorb more than those with 20 wt% volcanic ash (blue curves), even if there are evident overlaps between the curves. This means that the addition of volcanic ash partially hinders the absorption of water.

In detail, in all the sample groups, those fired at 950 °C absorbed the most water, although the values for these bricks were not significantly higher than for those fired at other temperatures. The bricks fired at 950 °C recorded the highest A_b values (Table 4). This trend was

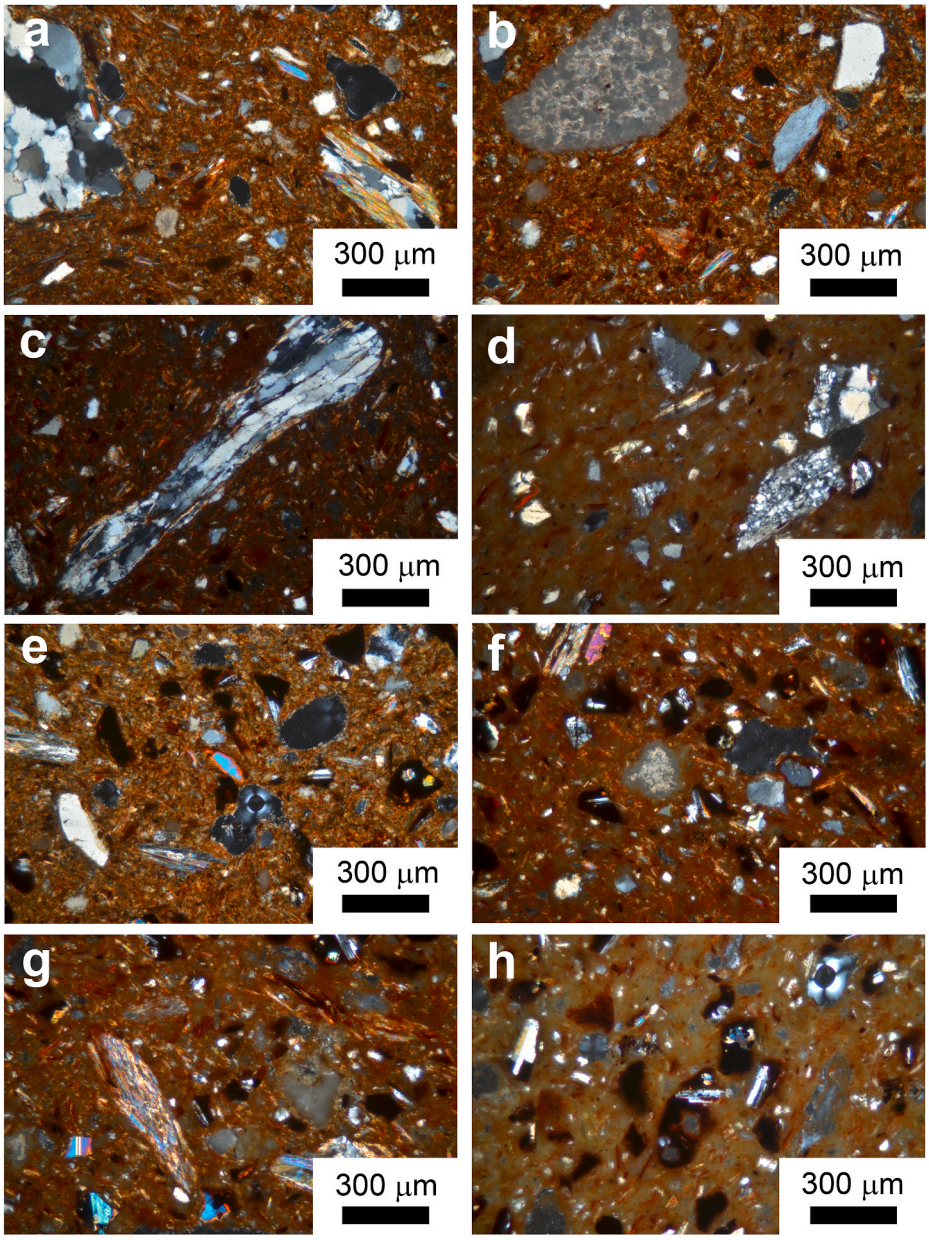

Fig. 4. Optical microscopy images of: a): general view of the VG800 brick in which gneiss fragments and isolated quartz and muscovite crystals can be identified in a reddish matrix; b) aspect of a partially decomposed calcite grain in the VG800 brick; c) aspect of a gneiss fragment in the VG950 brick in which the muscovite laminae have lost their typical birefringence, and the matrix has turned dark red; d) dark yellow matrix in the VG1100 brick in which quartz grains and small red hematite crystals can be identified; e) texture of the VGb800 brick in which irregular, black volcanic ash fragments are homogeneously distributed in the matrix. Plagioclase and pyroxene crystals can be identified in these ashes; f) calcite fragment in the VGb950 brick indicating partial decomposition on the edges of the crystal. At 950 °C the core of this carbonate is still birefringent; g) mica schist in VGb950 in which the muscovite laminae reach second order blue interference colour; h) a diffused brown halo has developed around the ash fragments in the VG1100 brick. For brick acronyms see Table 1. (For interpretation of the references to colour in this figure legend, the reader is referred to the Web version of this article.)

confirmed by the results obtained in the forced absorption test (A_f, Table 4 and part 2 of Fig. 6) and by the pore interconnection (Ax) values which are generally lower in samples fired at 950 °C. Conversely, an increase in Ax can be observed at 1100 °C, indicating that it is more difficult for the water to circulate between the pores, i.e. the tortuosity of the capillary network has increased [65]. This is caused by the vitrification of the matrix as demonstrated by microscopic observations. The drying index (Di) is almost identical in all the samples, if slightly slower at higher firing temperatures, a logical result given the poorer connection between the pores. The drying curves (part 3 of Fig. 6) show almost the same trend with an initial straight slope, slightly more pronounced in VGb1100. The saturation coefficient (S) follows the same trend as Di with a lower saturation as the firing temperature increases.

The porosity (P_o) varies between 34 and 40% and the samples fired at 800 °C, those that underwent the least mineralogical and textural changes, are also the least porous (Table 4). It is interesting to note that the addition of volcanic ash reduces the porosity at all firing temperatures. This reduction is higher in percentage terms in the bricks with a 20% ash content (porosity fell by between 5.9% and 8.7%) than with 10% (by between 2.8% and 6.4%). The volcanic ash increases the bulk density (ρ_a) and this is greater with higher ash contents. However, there is little variation in real density (ρ_r), a parameter that is closely related to the mineralogy of the brick, which was largely unaltered by the addition of volcanic ash with a silicatic composition, as was seen through PXRD (see Table 3).

In the porosimetric analysis, the bricks show unimodal pore size distribution. The increase in the firing temperature shifts the maximum peak towards larger pores, reducing the number of smaller ones. This shift is more noticeable in bricks without additives where the peak moves from 0.2 at 800 °C to 0.68 μm at 1100 °C (Fig. 7). At 950 °C the maximum peak is measured at 0.33 μm, i.e. closer to that for the bricks fired at 800 °C. This means that the greatest variations in the porous system occur above this temperature, perhaps due to vitrification. This result confirms those of the hydric tests, in that a reduction in pore interconnection is observed at 1100 °C (Ax, Table 4). The addition of volcanic ash alters the pore size distribution, while also reducing the displacement of the maximum peak towards larger dimensions. The changes are similar regardless of the volcanic ash content. In fact, the

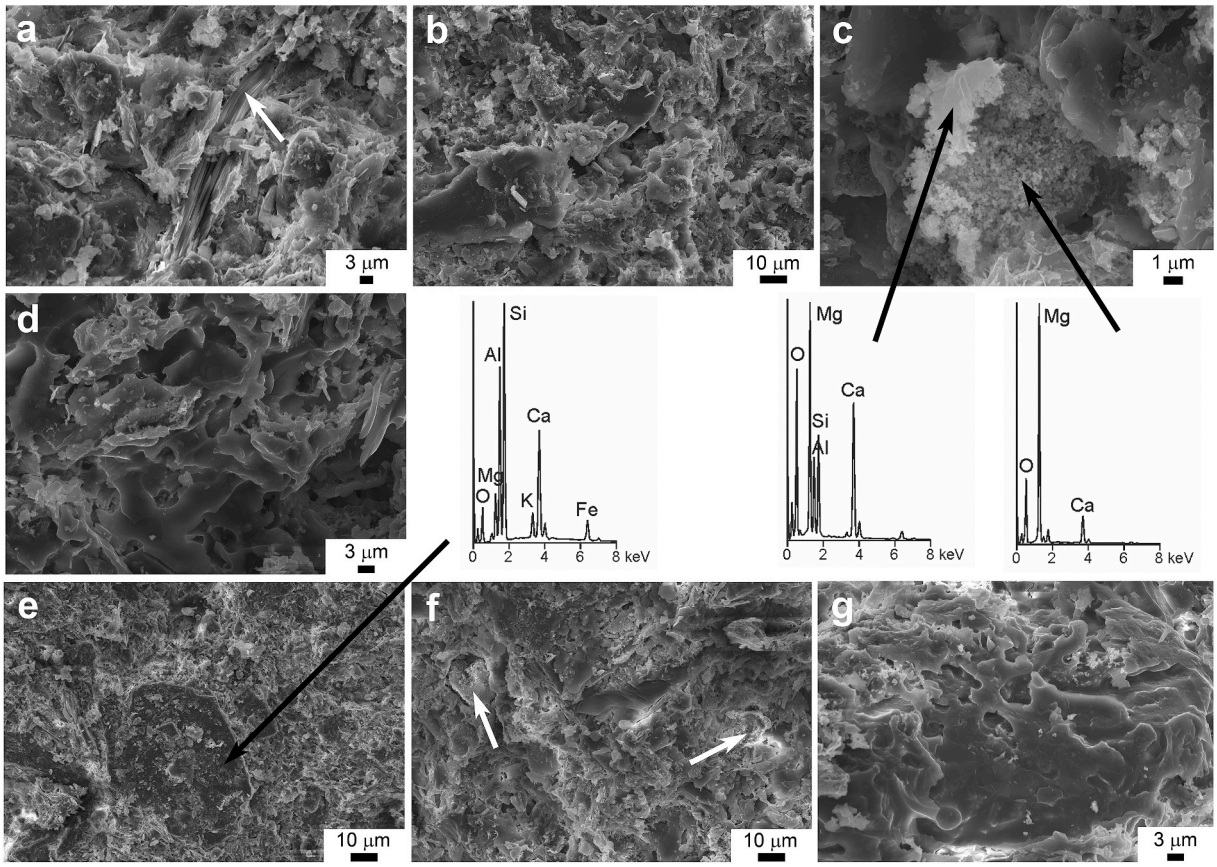

Fig. 5. FESEM secondary electron images and EDS spectra of the bricks made without additive (image a belongs to VG800, b and c to VG950, d to VG1100) and of those containing 20 wt% volcanic ash (image e belongs to VGb800, f to VGb950, g to VGb1100).

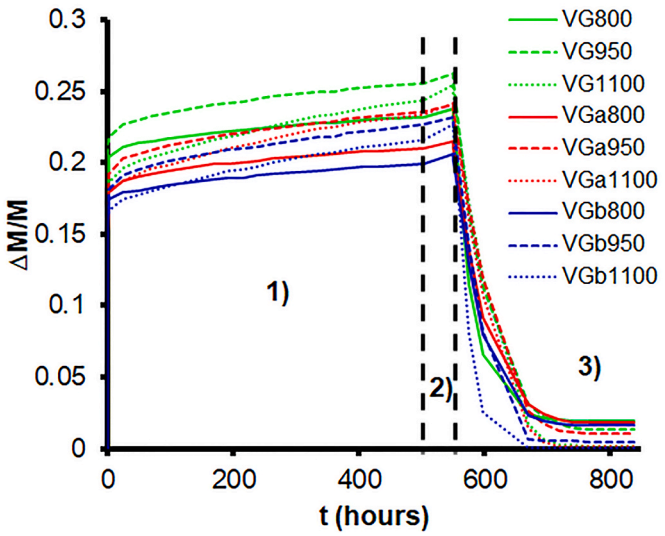

Fig. 6. 1) Water absorption at atmospheric pressure, 2) water absorption under vacuum and 3) drying curves for the bricks without additives (VG) and with added volcanic ash (VGa and VGb) fired at 800, 950 and 1100 °C. Weight variation (ΔM/M) versus time (in hours).

ash extends the range of the main family of pores to the right, i.e. towards the largest pores (Fig. 7). Moreover, it shifts the maximum peak of the bricks fired at 800 °C to 0.34 μm, reaching maximum displacement at 1100 °C (0.6 μm) albeit with little difference compared to 950 °C. The influence of volcanic ash on the pore system of the bricks is also highlighted by analysing the percentage of the porosity in four ranges indicated in Table 4. The bricks without residue show a gradual increase in porosity between 0.1 and 1 μm, while those between 0.01 and 0.1 μm show a decrease (Table 4). In bricks with volcanic ash, the pores between 0.1 and 1 μm are still the most abundant but the evolution in line with the firing temperature is different from that observed in the samples with no added ash. In fact, while this trend is maintained between 800 and 950 °C, at 1100 °C there is no further increase in the pores of between 0.1 and 1 μm, while those measuring more than 1 μm increase in number to over 16% (Table 4). At this temperature, the flux capacity of the residue enabled some of the pores in the 0.1–1 range to coalesce to form larger pores.

5.3.4. *Compactness and strength*

The increase in firing temperature augments the ultrasonic wave velocity in all the bricks regardless of whether or not they contain additives. The ultrasound velocity of the bricks studied in this work is normally lower than that of commercially available extruded bricks because less pressure is exerted on the raw material when making handmade bricks [66]. However, the values are in line with those recorded in other handmade bricks [67,68]. Table 5 shows that V_{P1} is always lower with respect to V_{P2} and V_{P3} because the phyllosilicates and planar rock fragments present in the raw material are oriented parallel to the surface on which pressure was exerted during the filling of the mould, i.e. perpendicular to the direction of wave propagation.

The bricks made without the additive are apparently more compact ($\overline{V_P}$ is higher, Table 5). This may be because the volcanic grains in the body of the brick cause the ultrasonic waves to scatter, so delaying their propagation [69,70]. The difference between V_{P1} and the other two velocities diminishes as the firing temperature increases and as more volcanic ash is added. This is because in the first case the bricks begin to

Table 4
Results of hydric and MIP tests on the bricks made without additives (VG) and with added 10 wt% (VGa) and 20 wt% volcanic ash (VGb). The standard deviation of each result of the hydric tests is indicated in brackets. A_b = free water absorption (%); A_f = forced water absorption (%); Ax = degree of pore interconnection; Di = drying index; S = saturation coefficient (%); P_o = open porosity (%); ρ_a = apparent density (g cm^{-3}); ρ_r = real density (g cm^{-3}). <0.01 = percentage of porosity lower than 0.01 μm; 0.01–0.1 = percentage of porosity between 0.01 μm and 0.1 μm; 0.1–1 = percentage of porosity between 0.1 μm and 1 μm; >1 = percentage of porosity higher than 1 μm (percentages determined by MIP).

	VG800	VG950	VG1100	VGa800	VGa950	VGa1100	VGb800	VGb950	VGb1100
A_b	23.19	25.59	24.35	21.05	23.58	23.36	19.93	22.65	21.58
	(0.25)	(0.19)	(0.08)	(0.51)	(0.25)	(0.29)	(0.22)	(0.20)	(0.29)
A_f	23.77	26.29	25.43	21.55	24.08	24.19	20.64	23.20	22.74
	(0.29)	(0.03)	(0.19)	(0.57)	(0.23)	(0.18)	(0.45)	(0.21)	(0.09)
Ax	2.47	2.66	4.25	2.31	2.08	3.43	3.42	2.40	5.06
	(0.16)	(0.84)	(0.81)	(0.20)	(0.12)	(0.57)	(1.14)	(0.65)	(1.58)
Di	0.90	0.89	0.89	0.91	0.90	0.89	0.91	0.90	0.89
	(0.000)	(0.002)	(0.003)	(0.004)	(0.004)	(0.005)	(0.000)	(0.002)	(0.000)
S	90.00	87.58	79.02	88.09	85.70	79.40	87.62	83.99	78.13
	(0.65)	(1.82)	(1.50)	(1.86)	(0.65)	(1.26)	(2.16)	(0.98)	(2.05)
P_o	37.91	40.84	39.95	35.50	38.69	38.85	34.62	38.05	37.60
	(0.31)	(0.29)	80.21)	(0.93)	(0.42)	(0.26)	(0.61)	(0.32)	(0.05)
ρ_a	1.59	1.55	1.57	1.65	1.61	1.61	1.68	1.64	1.65
	(0.01)	(0.01)	(0.00)	(0.00)	(0.00)	(0.00)	(0.01)	(0.00)	(0.00)
ρ_r	2.57	2.63	2.62	2.55	2.62	2.63	2.57	2.65	2.65
	(0.01)	(0.03)	(0.00)	(0.04)	(0.02)	(0.01)	(0.01)	(0.01)	(0.01)
<0.01	1.72	0.75	3.83	0.00	0.32	3.70	2.12	4.38	4.35
0.01–0.1	25.17	9.53	0.57	18.34	9.40	0.65	20.97	5.79	0.27
0.1–1	70.80	86.60	93.97	79.74	87.11	79.54	72.58	86.69	77.52
>1	2.31	3.12	1.63	1.92	3.17	16.11	4.33	3.14	17.86

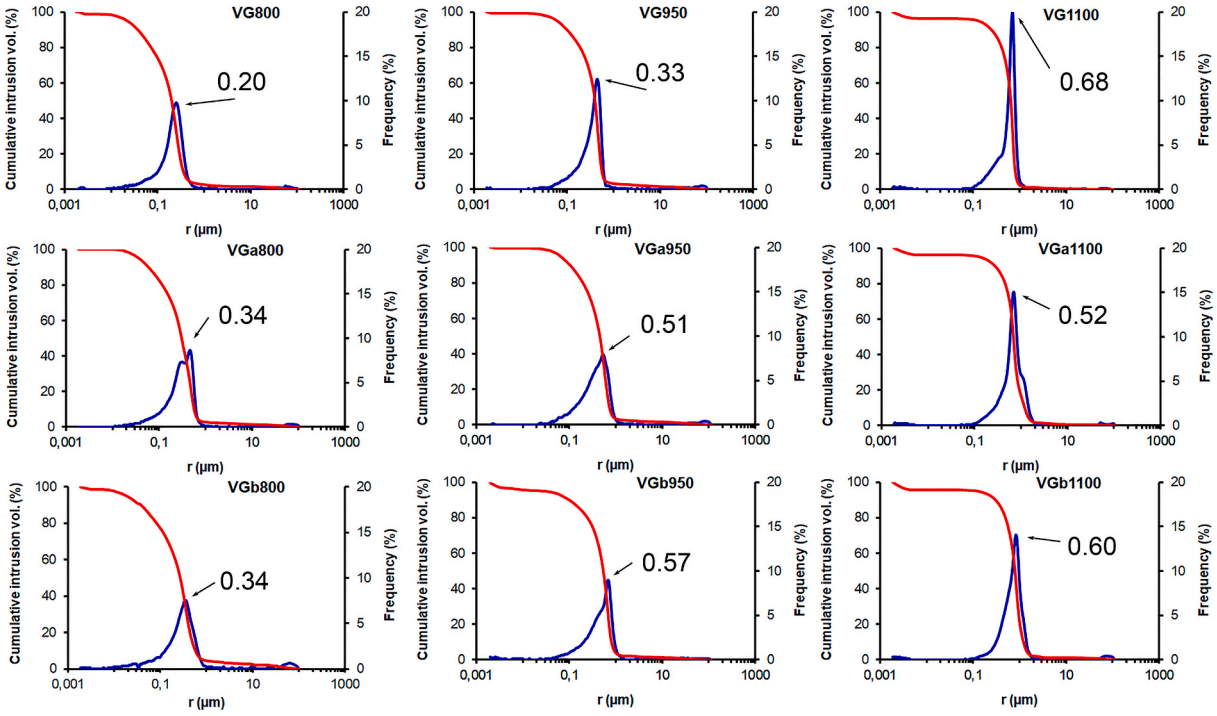

Fig. 7. Pore size distribution (blue) and cumulative mercury intrusion (red) curves of bricks without additive and with added volcanic ash. The radius (in μm) at the maximum peak in each porometric curve is indicated. Brick acronyms are indicated in Table 1. (For interpretation of the references to colour in this figure legend, the reader is referred to the Web version of this article.)

vitrify and the internal structure becomes more homogeneous; in the second case the bricks lose the marked orientation provided by the phyllosilicates due to the addition of irregular, non-planar particles. In both cases, the bricks become less anisotropic (ΔM, Table 5) and the higher the residue content, the lower the anisotropy.

Compressive strength (CS, Table 5) always increases in line with firing temperature and the greatest increase is between 950 and 1100 °C, when the bricks undergo the greatest textural changes, i.e. the most intense period of vitrification (see microscopic observations). The values obtained are clearly higher than in bricks used in historical buildings but lower than in modern ones due to the different manufacturing process [66,71,72]. It is interesting to note that the addition of volcanic ash reduces the compressive strength, and that the higher the ash content, the greater this reduction.

When the ultrasonic velocity of the bricks is compared to their resistance to uniaxial compression, there is an exponential relationship with a R^2 value of 0.81 (Fig. 8). The samples fired at 800 °C have the lowest $\overline{V_P}$ and CS values. The samples become more resistant (and the

Table 5
Compactness and strength of bricks determined by means of ultrasound and uniaxial compression tests, respectively. V_{P1}, V_{P2} and V_{P3} = P wave velocities along the three orthogonal brick surfaces (m/s). V_{P1} is the velocity perpendicular to the compaction plane of the raw material, while V_{P2} and V_{P3} are the velocities parallel to it; $\overline{V_P}$ = mean P wave velocity (m/s). The standard deviation σ is indicated in brackets; ΔM = anisotropy (%); CS = compressive strength (MPa). Brick acronyms are indicated in Table 1.

	V_{P1}	V_{P2}	V_{P3}	$\overline{V_P}$ (σ)	ΔM	CS
VG800	1581	2305	2044	1977 (42.67)	31.14	19.08
VG950	1894	2514	2292	2233 (18.39)	24.38	23.51
VG1100	2099	2510	2631	2413 (31.34)	22.09	31.79
VGa800	1564	2076	2095	1911 (62.52)	28.07	17.15
VGa950	1963	2271	2297	2177 (24.75)	17.55	21.35
VGa1100	2035	2408	2440	2295 (38.50)	15.27	31.33
VGb800	1748	2129	2152	2010 (44.82)	20.42	15.81
VGb950	1918	2259	2211	2130 (39.58)	15.24	18.08
VGb1100	2181	2410	2408	2333 (74.75)	10.57	25.87

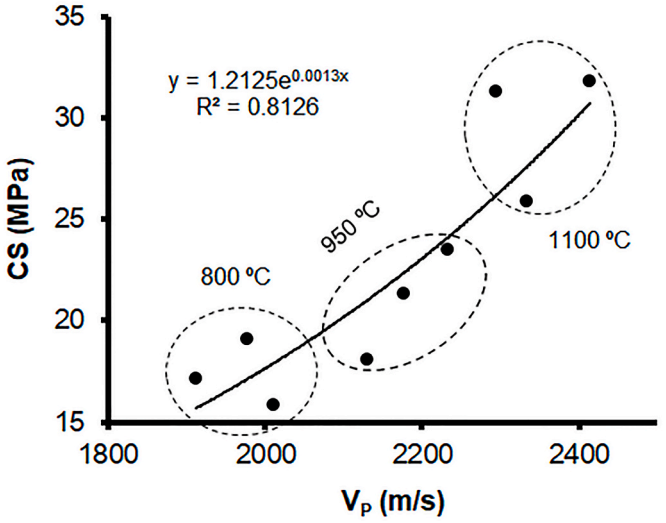

Fig. 8. Correlation between the mean P-wave velocity (in m/s) and compressive strength (in MPa). Dotted areas enclose the samples with different firing temperatures.

waves move more quickly) as the firing temperature increases. The exponential correlation between the two values indicates that as firing temperature increases and, above all, at 1100 °C, although there is a clear increase in both $\overline{V_P}$ and CS, CS increases much more sharply than $\overline{V_P}$. This is because compressive strength is more closely related to the enhanced bonding between particles, while wave propagation continues to be partially attenuated and refracted by the porous system and the grains.

5.3.5. *Spectrophotometry*

The addition of volcanic ash is responsible for the colour change in the bricks, even when only 10% of additive is used. The colour difference (ΔE) value is less than 3.5 (the threshold above which a colour change can be perceived by the human eye) in just two cases (Table 6). Moreover, most of bricks have ΔE >5, the limit above which people can clearly identify two colours as different [73]. The more volcanic ash added the greater the colour difference.

Table 6
Colour difference (ΔE) due to the addition of volcanic ash to the brick samples as compared to those made without additive.

	VGa800	VGa950	VGa1100	VGb800	VGb950	VGb1100
ΔE	3.04	6.13	3.26	5.60	6.95	6.22

As regards lightness (L*), if we analyse the unfired samples, the addition of volcanic ash reduces lightness values and this reduction is higher the greater the concentration of volcanic ash (L*, Fig. 9a). This is logical given the very dark colour of the added particles. By contrast, when the lightness (L*) of the fired samples is measured, the opposite trend is observed: the lightness value rises in all samples as the firing temperature increases. This means that the firing process has a more significant effect on L* than the addition of volcanic ash. On this question, Simonot and Elias [74] demonstrated that the structural changes in a material are responsible for the changes in its colour parameters. In our case, the bricks are vitrifying (see Figs. 4 and 5) and their surfaces are becoming more uniform, so favouring higher L* values. As for the chromatic parameters, the unfired samples have very similar a* and b* values with a greyish hue. Bricks turn orange in colour after firing at 800 and 950 °C and take on a yellowish hue at 1100 °C, mainly due to the crystallization of the hematite [75,76]. The chromatic coordinates (a* and b*) are influenced by the firing temperature and to a lesser extent by the amount of additive (Fig. 9b). The a* axis (which marks the red hue) varies over a wider range compared to the b* axis (which indicates yellow). It is interesting to note that firing temperature seems more closely linked to parameter a*, while volcanic ash content has closer links with parameter b*. In fact, the bricks fired at 1100 °C have the lowest a* values (Fig. 9b). This means that the red component of the colour is less intense and the bricks take on a darker colour (i.e. they turn towards the grey area in the CIEL*a*b* colour space). Lowering the firing temperature increases the a* values. The bricks with the most intense (most saturated) colour are those fired at 800 °C. If we compare the bricks made without additives with those that contain volcanic ash, higher b* values are always observed when no volcanic ash is present (Fig. 9b).

5.3.6. *Durability*

Fig. 10 shows the behaviour of the bricks when subjected to accelerated ageing by salt crystallization. During the first cycles (generally until cycles 5 or 6) there is an increase in weight due to the crystallization of sodium sulphate in the pores and fissures of the bricks. This increase is generally followed by a more or less marked decrease due to the loss of fragments. This weight loss may itself be followed by new gains, probably due to the precipitation of the salt in the newly formed fissures. With the naked eye, material loss occurs mainly along the edges of the samples. It is evident that all the bricks fired at 800 °C (with and without volcanic ash) gain more weight than those fired at 950 and 1100 °C. This seems to be related to pore size, as pores measuring less than 0.1 μm are more abundant at lower firing temperatures (see Table 4). On this question, Scherer [77] showed that crystallization stress, which led to stone damage, depends among other factors on pore size and that stress is higher in smaller pores. As a consequence, VG800 is the sample that undergoes greater fluctuations in weight (with a marked fall in cycle 12) compared to the other two bricks fired at 800 °C, which contained added volcanic ash. Of these two bricks (VGa800 and VGb800), the bricks with the highest volcanic ash content gain less weight (Fig. 10). This trend is also maintained at 950 and 1100 °C, where the VGb samples are always the ones that gain least weight. This indicates that the addition of this waste product does improve the durability of the bricks. Although the increase in temperature reduces the entry of salts into the porous system, the gradual vitrification of the bricks also causes sudden weight losses due to the stronger bond between the particles. In fact, brick decay ranges from powdering at 800 °C to crumbling at 950 and 1100 °C.

6. Conclusions

In this paper, the addition of volcanic ash from Mount Etna (Eastern Sicily, Italy) to the clayey mix used in brick production was investigated, in order to assess whether physically and mechanically efficient building

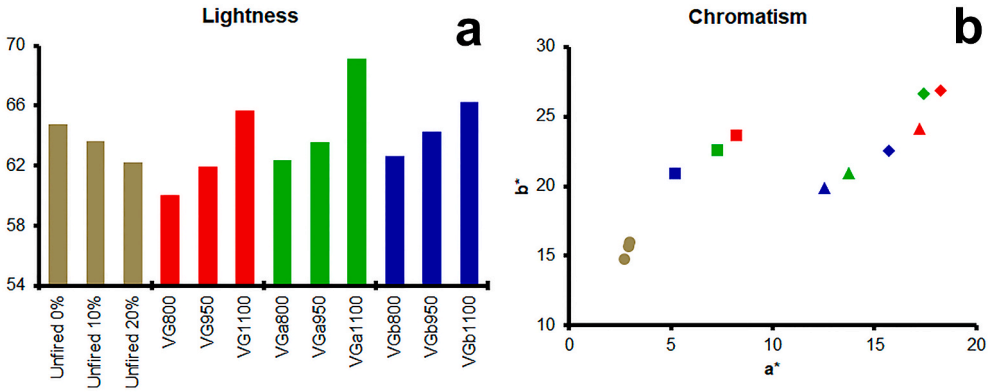

Fig. 9. Lightness (a) and chromaticity (b) of unfired (grey) and fired bricks without additives (red), with added 10 wt% volcanic ash (green) and with added 20 wt% (blue). The circles represent the unfired bricks; the diamonds represent those fired at 800 °C; the triangles represent those fired at 950 °C; the squares represent those fired at 1100 °C. (For interpretation of the references to colour in this figure legend, the reader is referred to the Web version of this article.)

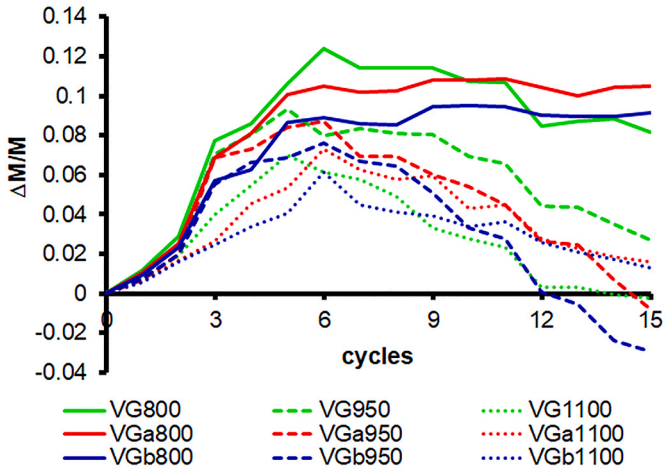

Fig. 10. Weight variation in bricks made without additives (VG) and with added volcanic ash (VGa and VGb) over 15 salt crystallization test cycles. Each curve represents the mean of three measurements.

materials could be made with this mixture. To this end, a range of samples were prepared by firing the raw material (which was rich in quartz, phyllosilicates and carbonates) at 800, 950 and 1100 °C. This caused changes in the mineralogy and the texture, which were manifested in the appearance of new silicate phases, such as gehlenite, mullite, diopside and Ca-plagioclase and the vitrification of the matrix. The addition to the raw material of 10 and 20 wt% volcanic ash, in the same state as collected, i.e. without sieving or crushing, reduced the amount of kneading water required in the production process by up to 14%. This residue also delayed the development of new phases during firing and was easily distinguishable under the optical and scanning electron microscopes in bricks fired at 800 °C due to its irregular morphology. At higher temperatures, the ash particles began to melt within the matrix and bonded well into a partially vitrified brick structure. As the firing temperature increased, the mineralogical and textural differences between the bricks made with and without ash reduced.

From a physical point of view, the addition of volcanic ash reduced the porosity of the bricks, a trend that intensified as the ash content increased. The gradual vitrification of the bricks resulted in coalescence between the pores and in the shift of the porometric curve towards larger pores, especially in the presence of volcanic ash, where the number of pores of over 1 μm increased. Vitrification was also responsible for decreasing the degree of interconnection between the pores, especially at 1100 °C. The bricks became more compact and their compressive strength increased as the firing temperature augmented. The addition of volcanic ash reduced both compactness and strength. In any case, the values obtained remained above those recommended for building work with ceramic materials [78].

The addition of volcanic ash caused a perceivable change in colour in almost all the bricks. However, they retained an orange colour which tended towards yellow in the samples fired at 1100 °C.

The bricks made with volcanic ash were less subject to decay due to salt crystallization and the most resistant bricks were those with the highest residue content. The firing temperature also improved the durability of the bricks, especially at 1100 °C, thanks to the stronger bond between the particles due to vitrification.

Table 7 summarizes the performance of the nine types of bricks by selecting six parameters from the petrographic, physical and ageing analyses conducted in this research. These six parameters were as follows: the development and amount of new phases and texture birefringence characterized by powder X-ray diffraction and polarized optical microscopy, the degree of pore interconnection and open porosity both calculated by hydric tests, the compactness measured with ultrasounds, the compressive strength calculated using mechanical stress tests and, finally, the resistance to decay assessed by salt crystallization. The bricks were awarded a score from 1 (worst performance) to nine (best performance) based on their performance in each of the above tests. The average score obtained by each sample for the six parameters was then calculated. These scores show that the quality of the bricks improves as the firing temperature increases due to vitrification. The addition of volcanic ash does not improve the petrophysical properties of the bricks fired at low temperatures, but at 950 °C and especially at 1100 °C the bricks melted at least partially, blending better with the clayey matrix,

Table 7
Summary of the performance of the nine types of brick in petrographic, physical and durability terms. Performance was measured on a scale from 1 to 9 with 1 being the worst and 9 the best. Legend: Min. = development of new mineral phases + texture birefringence; Ax = degree of pore interconnection; P_o = open porosity; $\overline{V_P}$ = mean P wave velocity; CS = compressive strength; Salt = resistance to salt crystallization. Bricks acronyms are indicated in Table 1.

	Min.	Ax	P_o	$\overline{V_P}$	CS	Salt	Mean
VG800	4	6	6	2	4	1	3.8
VG950	6	5	1	6	6	4	4.7
VG1100	9	2	2	9	9	7	6.3
VGa800	1	8	8	1	2	2	3.7
VGa950	3	9	4	5	5	5	5.2
VGa1100	9	3	3	7	8	9	6.5
VGb800	1	4	9	3	1	3	3.5
VGb950	5	7	5	4	3	6	5.0
VGb1100	9	1	7	8	7	9	6.8

so becoming more resistant and durable.

This study shows that volcanic ash has great potential for reuse in the ceramic industry. Given that there are volcanic ash deposits all over the world in places with current or past volcanic activity, this ash should no longer be treated as waste to be disposed of in landfills, and should instead be viewed as a resource in the production of new efficient bricks that can contribute to the development of a circular economy.

Declaration of competing interest

The authors declare that they have no known competing financial interests or personal relationships that could have appeared to influence the work reported in this paper.

Acknowledgements

This study was funded by Junta de Andalucía Research Group RNM179 and by Research Project MAT2016-75889-R. Funding for open access charge: Universidad de Granada/CBUA. I thank Cerámica Castillo Siles for providing the raw material used to prepare and fire the bricks and the Centro de Instrumentación Científica (CIC, University of Granada) for its assistance with the granulometry, XRF, TG-DSC and FESEM analyses. I am grateful to Nigel Walkington for his assistance in revising the English text of the manuscript.

References

[1] A. Rittmann, Les volcans et leur activité. French Edition from the 2nd original edition, Masson & Cie, Paris, 1963.
[2] R.A. Corsaro, L. Miraglia, The transition from Summit to flank activity at Mt. Etna, Sicily (Italy): influences from the petrology of products erupted in 2007-2009, J. Volcanol. Geoth. Res. 275 (2014) 51–60.
[3] S. Branca, M. Coltelli, G. Groppelli, Geological evolution of a complex basaltic stratovolcano: Mount Etna, Italy. Ital. J. Geosci. 130 (2011) 306–317.
[4] R. Romano, C. Sturiale, The historical eruptions of Mt. Etna (Volcanological data), Mem. Soc. Geol. It. 23 (1982) 75–97.
[5] S. Branca, M. Coltelli, G. Groppelli, F. Lentini, Geological map of Etna volcano, 1: 50000 scale, Ital. J. Geosci. 130 (2011) 265–291.
[6] C. Ferlito, R. Cristofolini, Geologia dell'area sommitale etnea, Boll. Accademia Goenia Sci. Nat. 22 (1989) 357–380.
[7] S. Barsotti, D. Andronico, A. Neri, P. Del Carlo, P.J. Baxter, W.P. Aspinall, T. Hincks, Quantitative assessment of volcanic ash hazards for heath and infrastructure at Mt. Etna (Italy) by numerical simulation, J. Volcanol. Geoth. Res. 192 (2010) 85–96.
[8] L. Hayes, T.M. Wilson, C. Magill, Tephra fall clean-up in urban environments, J. Volcanol. Geoth. Res. 304 (2015) 359–377.
[9] C.J. Horwell, P.J. Baxter, The respiratory health hazards of volcanic ash: a review for volcanic risk mitigation, Bull. Volcanol. 69 (2006) 1–24.
[10] A.I. Tesone, R.M. Lasagni Vitar, J. Tau, G.A. Maglione, S. Llesuy, D.R. Tasat, A. Berra, Volcanic ash from Puyehue-Cordón Caulle volcanic complex and Calbuco promote a differential response of pro-inflammatory and oxidative stress mediator son human conjunctival epithelial cells, Environ. Res. 167 (2018) 87–97.
[11] F. Bardelli, G. Giuli, F. Di Benedetto, P. Castagliola, G. Montegrossi, V. Rimondi, M. Romanelli, L.A. Pardi, G. Barone, P. Mazzoleni, Spectroscopic study of volcanich ashes, J. Hazard Mater. 400 (2020) 1–11, 123213.
[12] G. Barone, G. De Giudici, D. Gimeno, G. Lanzafame, F. Podda, C. Cannas, A. Giuffrida, M. Barchitta, A. Agodi, P. Mazzoleni, Surface reactivity of Etna volcanic ash and evaluation of health risks, Sci. Total Environ. 761 (2021), 143248.
[13] D. Andronico, S. Scollo, S. Caruso, A. Cristaldi, The 2002-03Etna explosive activity: tephra dispersal and features of the deposits, J. Gephys. Res. 113 (2008) 1–16. B04209.
[14] R. Siddique, Effect of volcanic ash on the properties of cement paste and mortar, Resour. Conserv. Recycl. 56 (2011) 66–70.
[15] L. Contrafatto, Recycled Etna volcanic ash for cement, mortar and concrete manufacturing, Construct. Build. Mater. 151 (2017) 704–713.
[16] C. Finocchiaro, G. Barone, P. Mazzoleni, C. Leonelli, A. Gharzouni, S. Rossignol, FT-IR study of early stages of alkali activated materials based on pyroclastic deposits (Mt. Etna, Sicily, Italy) using two different alkaline solutions, Construct. Build. Mater. 262 (2020) 1–11, 120095.
[17] H.K. Tchakoute, A. Elimbi, E. Yanne, C.N. Djangang, Utilization of volcanic ashes for the production of geopolymers cured at ambient temperature, Cement Concr. Compos. 38 (2013) 75–81.
[18] P.N. Lemougna, K.T. Wang, Q. Tang, A.N. Nzeukou, N. Billong, U. Chinje Melo, C. Xue-min, Review on the use of volcanic ashes for engineering applications, Resour. Conserv. Recycl. 137 (2018) 177–190.
[19] A. Al-Fakih, B.S. Mohammed, M. Shahir Liew, E. Nikbakht, Incorporation of waste materials in the manufacture of masonry bricks: an update review, J. Build. Eng. 21 (2019) 37–54.
[20] L. Zhang, Production of bricks from waste materials - a review, Construct. Build. Mater. 47 (2013) 643–655.
[21] N. Saenz, E. Sebastián, G. Cultrone, Analysis of tempered bricks: from raw material and additives to fired bricks for use in construction and heritage conservation, Eur. J. Mineral 31 (2019) 301–312.
[22] P. Muñoz Velasco, M.P. Morales Ortíz, M.A. Mendívil Giró, L. Muñoz Velasco, Fired clay bricks manufactured by adding wastes as sustainable construction material, A review. Constr. Build. Mater. 63 (2014) 97–107.
[23] R.J. Galán Arboledas, M.T. Cotes Palomino, C. Martínez García, J.M. Moreno Maroto, M. Uceda Rodríguez, S. Bueno, Ternary diagrams as a tool for developing ceramic materials from waste: relationship between technological properties and microstructure, Environ. Sci. Pollut. R. 26 (2019) 35574–35587.
[24] T. Gillot, I. Cojan, F. Haurine, C. Poirier, M.A. Bruneaux, Demonstrating the influence of sediment source in dredged sediment recovery for brick and tile production, Resour. Conserv. Recycl. 171 (2021), 105653.
[25] H.V. Cabadas Báez, B. Solís Castillo, E. Solleiro-Rebolledo, S. Sedov, D. Leonard, K. Teranishi Castillo, R. Liendo Stuardo, O. Korneychik, Reworked volcaniclastic deposits from the Usumacinta river, Mexico: a serendipitous source of volcanic glass in Maya ceramics, Geoarchaeology 32 (2017) 382–399.
[26] V. Morra, A. De Bonis, C. Grifa, A. Langella, L. Cavassa, R. Piovesan, Minero-petrographic study of cooking ware and pompeian red ware (rosso pompeiano) from Cuma (Southern Italy), Archaeometry 55 (2013) 852–879.
[27] M.F. Serra, M.S. Conconi, G. Suarez, E.F. Aglietti, N.M. Rendtorff, Volcanic ash as flux in clay based triaxial ceramic materials, effect of the firing temperature in phases and mechanical properties, Ceram. Int. 41 (2015) 6169–6177.
[28] D.H. Vu, K.S. Wang, B. Xuan Nam, B. Hoang Bac, T.C. Chu, Preparation of humidity-controlling porous ceramics from volcanic ash and waste glass, Ceram. Int. 37 (2011) 2845–2853.
[29] C.M. Belfiore, C. Amato, A. Pezzino, M. Viccaro, An end of waste alternative for volcanic ash: a resource in the manufacture of ceramic tiles, Construct. Build. Mater. 263 (2020) 1–15, 120118.
[30] A. Ruiz Bustos, J. Fernández, J. Morales, J. Rodríguez Fernández, J.A. Vera, Los materiales Plio-Pleistocenos del borde norte de la depresión de Granada, Estud. Geol. 46 (1990) 270–290.
[31] H. Corbí, C. Lancis, F. García-García, J.A. Pina, J.M. Soria, J.E. Tent Manclús, C. Viseras, Updating the marine biostratigraphy of the Granada basin (central betic Cordillera). Insight for the late miocene palaeogeographic evolution of the Atlantic-mediterranean seaway, Geobios 45 (2012) 249–263.
[32] J.M. Soria, J. Fernández, C. Viseras, Late miocene stratigraphy and paleogeographic evolution of the intramontane Guadix basin (central betic Cordillera, Spain): implications for an Atlantic-mediterranean connection, Palaeogeogr. Palaeoclimatol. Palaeoecol. 151 (1999) 255–266.
[33] M.L. Calvache, C. Viseras, Long-term control mechanisms of stream piracy processes in southeast Spain, Earth Surf. Process. Landforms 22 (1997) 93–105.
[34] R.T. Laird, M. Worcerster, The inhibiting of lime blowing, Trans. Br. Ceram. Soc. 55 (1956) 545–563.
[35] G. Bruton, Vapour glycolation, Am. Mineral. 40 (1955) 124–126.
[36] D.M. Moore, R.C. Reynolds, X-ray Diffraction and the Identification and Analysis of Clay Minerals, Oxford University Press, Oxford, 1989.
[37] UNE-EN 13755, Natural Stone Test Methods. Determination of Water Absorption at Atmospheric Pressure, AENOR, Madrid, Spain, 2008.
[38] NORMAL 29/88, Misura dell'indice di asciugamento (drying index), ICR-CNR, Rome, Italy, 1988.
[39] G. Cultrone, M.J. de la Torre, E. Sebastián, O. Cazalla, Evaluation of bricks durability using destructive and nondestructive methods (DT and NDT), Mater. Construcción 53 (2003) 41–59.
[40] Rilem, Recommended test to measure the deterioration of stone and to assess the differences of treatment methods, Mater. Struct. 13 (1980) 175–253.
[41] R.M. Esbert, J. Ordaz, F.J. Alonso, M. Montoto, Manual de Diagnosis y Tratamiento de Materiales Pétreos y Cerámicos, Col.legi d'Aparelladors i Arquitects Tècnics de Barcelona, Barcelona, Spain, 1997.
[42] E. Molina, G. Cultrone, E. Sebastián, F.J. Alonso, Evaluation of stone durability using a combination of ultrasound, mechanical and accelerated ageing tests, J. Geophys. Eng. 10 (2013), 035003.
[43] ASTM D2845, Standard Test Method for Laboratory Determination of Pulse Velocities and Ultrasonic Elastic Constant of Rock, American Society for Testing and Materials, USA, 2005.
[44] UNE-EN 1926, Natural Stone Test Methods. Determination of Uniaxial Compressive Strength, AENOR, Madrid, Spain, 2007.
[45] UNE-EN 15886, Conservation of Cultural Property. Test Methods. Colour Measurement of Surfaces, AENOR, Madrid, Spain, 2011.
[46] UNE-EN 12370, Natural Stone Test Methods. Determination of Resistance to Salt Crystallization, AENOR, Madrid, Spain, 2020.
[47] Y. Maniatis, M.S. Tite, Technological examination of neolithic-bronze age pottery form central and southeast Europe and from the near East, J. Archaeol. Sci. 8 (1981) 59–76.
[48] M.J. Le Bas, R.W. Le Maitre, A. Streckeisen, B. Zanettin, A chemical classification of volcanic rocks based on the Total Alkali-Silica diagram, J. Petrol. 27 (1986) 745–750.
[49] R.A. Corsaro, M. Pompilio, Magma dynamics in the shallow plumbing system of Mt. Etna as recorded by compositional variations in volcanics of recent summit activity (1995-1999), J. Volcanol. Geoth. Res. 137 (2004) 55–71.

[50] J.C. Tanguy, Tholeiitic basalt magmatism of Mount Etna and its relations with the alkaline series, Contrib. Mineral. Petrol. 66 (1978) 51–67.
[51] R. Cristofolini, R. Romano, Petrologic features of the Etnean volcanic rocks, Mem. Soc. Geol. It. 23 (1982) 99–115.
[52] R.A. Corsaro, N. Métrich, Chemical heterogeneity of Mt. Etna magmas in the last 15 ka. Inferences on their mantle sources, Lithos 252–253 (2006) 123–134.
[53] J.M. Martin, M. Ortega Huertas, J. Torres Ruiz, Genesis and evolution of strontium deposits of the Granada basin (Southeastern Spain): evidence of diagenetic replacement of a stromatolite belt, Sediment. Geol. 39 (1984) 281–298.
[54] E. Lopez Capel, S.P. Sohi, J.L. Gaunt, D.A.C. Manning, Use of thermogravimetry-Differential Scanning Calorimetry to characterize modelable soil organic matter fractions, Soil Sci. Soc. Am. J. 69 (2005) 136–140.
[55] G. Cultrone, F.J. Carrillo Rosua, Growth of metastable phases during brick firing: mineralogical and microtextural changes induced by the composition of the raw material and the presence of additives, Appl. Clay Sci. 185 (2020) 1–11, 105419.
[56] S. Guggenheim, A.F.K. Van Groos, Baseline studies of the Clay Minerals Society source clays: thermal analysis, Clay Clay Miner. 49 (2001) 433–443.
[57] C. Rodriguez Navarro, G. Cultrone, A. Sánchez Navas, E. Sebastián, TEM study of mullite growth after muscovite breakdown, Am. Mineral. 88 (2003) 713–724.
[58] R.S. Boynton, Chemistry and Technology of Lime and Limestone, second ed., Wiley, New York, 1980.
[59] C. Rodriguez Navarro, E. Ruiz Agudo, A. Luque, A.B. Rodriguez Navarro, M. Ortega Huertas, Thermal decomposition of calcite: mechanisms of formation and textural evolution of CaO nanocrystals, Am. Mineral. 94 (2009) 578–593.
[60] A. De Bonis, G. Cultrone, C. Grifa, A. Langella, V. Morra, Clays from the bay of Naples (Italy): new insight on ancient and traditional ceramics, J. Eur. Ceram. Soc. 34 (2014) 3229–3244.
[61] F. García Labiano, A. Abad, L.F. de Diego, P. Gayán, J. Adánez, Calcination of calcium-based sorbents at pressure in a broad range of CO_2 concentrations, Chem. Eng. Sci. 57 (2002) 2381–2393.
[62] L. Maritan, L. Nodari, C. Mazzoli, A. Milano, U. Russo, Influence of firing conditions on ceramic products: experimental study on clay rich in organic matter, Appl. Clay Sci. 31 (2006) 1–15.
[63] A. Escardino, J. García Ten, M. Soriano, Study of calcite decomposition during wall tile firing, in: Cámara Oficial de Comercio, Industria y Navegación de Castellón (Ed.), IX World Congress on Ceramic Tile Quality, 12-15 February 2006, 2006, pp. 265–278. Castellón (Spain).
[64] C. Rodriguez Navarro, K. Kudlacz, E. Ruiz Agudo, The mechanism of thermal decomposition of dolomite: new insights from 2D-XRD and TEM analyses, Am. Mineral. 97 (2012) 38–51.
[65] C. Hall, W.D. Hoff, Water Transport in Brick, Stone and Concrete, Taylor & Francis, New York, 2002.
[66] S. Noor-E-Khuda, F. Albermani, Mechanical properties of clay masonry units: destructive and ultrasonic testing, Construct. Build. Mater. 219 (2019) 111–120.
[67] G. Cultrone, E. Sebastián, K. Elert, M.J. de la Torre, O. Cazalla, C. Rodriguez Navarro, Influence of mineralogy and firing temperature on the porosity of bricks, J. Eur. Ceram. Soc. 24 (2004) 547–564.
[68] M. Canbaz, U. Albayrak, Properties of ancient style handmade clay bricks using bottom ash, Anadolu University J. Sci. Tech. A- Appl. Sci. Eng. 19 (2018) 104–113.
[69] J. Martínez Martínez, D. Benavente, M.A. García del Cura, Petrographic quantification of brecciated rocks by image analysis. Application to the interpretation of elastic wave velocities, Eng. Geol. 90 (2007) 41–54.
[70] J. Martínez Martínez, D. Benavente, M.A. García del Cura, Spatial attenuation: the most sensitive ultrasonic parameter for detecting petrographic features and decay processes in carbonatic rocks, Eng. Geol. 119 (2011) 84–95.
[71] Y. Endo, K. Yamaguchi, T. Hanazato, C. Mishra, Characterisation of mechanical behaviour of masonry composed of fired bricks and earthen mortars, Eng. Fail. Anal. 109 (2020), 104280.
[72] R. Capozucca, E. Magagnini, Brickwork wall models strengthened with diagonal and horizontal GFRP strips, Compos. Struct. 271 (2021), 114062.
[73] W.S. Mokrzycki, M. Talot, Colour difference ΔE. A survey, Mach. Graph. Vis. 20 (2011) 383–411.
[74] L. Simonot, M. Elias, Color change due to surface state modification, Color Res. Appl. 28 (2002) 45–49.
[75] R. Kreimeyer, Some notes on the firing colour of clay bricks, Appl. Clay Sci. 2 (1987) 175–183.
[76] A. De Bonis, G. Cultrone, C. Grifa, A. Langella, A.P. Leone, M. Mercurio, V. Morra, Different shades of red: the complexity of mineralogical and physicochemical factors influencing the color of ceramics, Ceram. Int. 43 (2017) 8065–8074.
[77] G.W. Scherer, Crystallization in pores, Cement Concr. Res. 29 (1999) 1347–1358.
[78] RL-88, Pliego general de condiciones para recepción de los cerámicos en las obras de construcción, Ministerio de Obras Públicas, Transportes y Medio Ambiente, Madrid, Spain, 1988.
[79] D.L. Whitney, B.W. Evans, Abbreviations for names of rock-forming minerals, Am. Mineral. 95 (2010) 185–187.